



# Novel ZnO-NiO-graphene-based sorbents for removal of hydrogen sulfide at intermediate temperature

J.M. Sánchez-Hervás<sup>a,\*</sup>, M. Maroño<sup>a</sup>, R. Fernández-Martínez<sup>b</sup>, I. Ortiz<sup>a</sup>, R. Ortiz<sup>a</sup>, M. B. Gómez-Mancebo<sup>b</sup>

<sup>a</sup> CIEMAT, Sustainable Thermochemical Valorization Unit, Energy Department, Spain

<sup>b</sup> CIEMAT, Spectroscopy Unit, Technology Department, Spain

## ARTICLE INFO

### Keywords:

Gas cleaning  
Desulfurization  
Sorbent  
ZnO-NiO-rGO composite  
Graphene  
Syngas

## ABSTRACT

When syngas is upgraded to bio-refinery products, hydrogen sulfide removal is necessary to prevent corrosion of equipment and avoid poisoning of sulfur sensitive catalysts. Technologies relying on sorbents working in the 300–500 °C temperature range are desirable for better process integration. In this work, a new family of reduced graphene ZnO-NiO sorbents, Zn-Ni-rGO, were synthesized by non-expensive and easily replicable scalable methods and studied for the first time for hydrogen sulfide reactive adsorption. Preparation was based on the Hummers & the improved Tour methods followed by addition of Zn(NO<sub>3</sub>), Ni(NO<sub>3</sub>), hydrothermal reduction and annealing. As obtained as well as post-reaction rGO-NiO-ZnO sorbents were characterized by XRF, XRD and N<sub>2</sub> adsorption at -196 °C. The performance of the sorbents for fixed bed desulfurization was determined at lab-scale (P = 10 bar, T = 400 °C, GHSV = 3500 h<sup>-1</sup>) on a gas stream containing 9000 ppmv of H<sub>2</sub>S/N<sub>2</sub>. The sorbents showed better hydrogen sulfide removal capacity than the commercial one studied for comparison, what makes them a potential candidate for gas cleaning in the syngas-related sectors.

## 1. Introduction

Desulfurization of raw gasification gases was a relevant topic during the 80–90 s, associated mainly with Integrated Gasification in Combined Cycle IGCC. Currently, there is a renewed surge in comprehensive sulfur removal due to the role of syngas for production of second generation biofuels, both gaseous and liquids. The main driver is related to preventing poisoning of sulfur sensitive catalysts when upgrading syngas to biofuels. Technologies relying on regenerable sorbents working in the 300–500 °C temperature range are desirable for better process integration.

Doing a brief historic review, implemented sulfur removal technologies coupled to IGCC were based on proven technologies from refinery processes. They mostly relied on wet scrubbing at low temperature, using chemical solvents. In parallel a good number of R&D studies were devoted to developing technologies for sulfur removal at warm temperature. Among the many sorbents thermodynamically feasible for sulfur removal, iron and zinc oxides and titanates reached a higher development stage.

More recent reviews on syngas desulfurization show that most

processes still rely on the experience and development gained in those decades and stress that high temperature gas cleaning is the best option when syngas is intended for (bio-)fuels production [1,2].

Zinc-oxide based commercial regenerable sorbents, e.g. Z-Sorb™ and S-Zorb™, have demonstrated to provide full removal of hydrogen sulfide from thermochemical conversion processes and specifically from gasification gases [3,4]. Experimental results at pilot scale proved the sulfur uptake capacity (removal of H<sub>2</sub>S) of Z-Sorb™ at high temperature (300–600 °C) and over a wide pressure range (1–20 bar) under numerous operation conditions and reaction atmospheres (from H<sub>2</sub>S/N<sub>2</sub> to full syngas) defining the effect of the main process parameters (space velocity, temperature, pressure), [5], suitable regeneration conditions and the application to IGCC cases [6].

In addition to the current investigations linked to applications and needs imposed on syngas desulfurization, related to stricter levels of sulfur removal to reach the tolerance of catalysts for biofuels production, the search for novel sorbents and particularly of new supports is a topic of intense research. In ECOSGAS, the project which funded the activities and results presented in this paper, graphene was investigated as a potential candidate.

\* Corresponding author.

E-mail address: [josemaria.sanchez@ciemat.es](mailto:josemaria.sanchez@ciemat.es) (J.M. Sánchez-Hervás).

Graphene, a new generation material, is an allotrope of elemental carbon which has motivated vast scientific interest due to its outstanding properties. It is a two-dimensional honeycomb single layer crystal lattice formed by tightly packed sp<sup>2</sup> bonded carbon atoms [7,8]. Due to its unique structure, carbon atoms form an excellent electron carrier space. In addition, graphene has high specific surface area (up to 2620 m<sup>2</sup>.g<sup>-1</sup>), excellent mechanical properties such as Young's modulus (1 TPa) and intrinsic strength (130 GPa), thermal conductivity (above 3000 W.m.K<sup>-1</sup>) and electrical conductivity (above 200000 cm<sup>2</sup>.V<sup>-1</sup>.s<sup>-1</sup>) [9–12].

Utilization of graphene-related materials is the focus of research activity in many fields. Among them, their use as support frameworks for functional nanoparticles is a fertile research area for a wide variety of applications, which include nanoelectronics, supercapacitors, fuel-cells, batteries, photovoltaics, catalysis, gas sorption, separation and storage, and sensing [13]. Hybrid materials based on inorganic nanoparticles and graphene or its hydrophilic derivative, graphene oxide (GO), have been shown to significantly boost the functional performance in a wide range of applications such as heterogeneous, electro and photocatalysis [14,15], CO<sub>2</sub> absorption [16] and gas sensing [17]. Among the different graphene-related materials, the chemically reduced graphene oxide, rGO, which is obtained from graphite precursors through oxidation-mechanical exfoliation-reduction processes, possesses the advantages of low cost and bulk quantity production, since it requires relatively inexpensive equipment and graphene-based materials can form colloidal stable suspensions which are important to facilitate the assembly of macroscopic structures as well as to integrate with other materials by simple and cheap solution processes.

As pointed out by Faye et al. 2016, [18] the high affinity of graphene for H<sub>2</sub>S makes it a potential adsorbent for separating H<sub>2</sub>S from gas streams. S atoms can get bonded to graphene during adsorption and at high temperatures, H<sub>2</sub>S dissociates at graphene defects leading to H<sub>2</sub> desorption with S atoms remaining on graphene.

Daraee et al., 2020 [19] looked into the adsorption of hydrogen sulfide at mid temperature (200–220 °C) onto TiO<sub>2</sub>/graphene oxide (TiO<sub>2</sub>/GO) nanohybrids, showing that the increase in the temperature had a positive effect on the adsorption of H<sub>2</sub>S.

H<sub>2</sub>S adsorption at mid temperature (150 °C) was also performed by Bhorja et al, 2020, [20] onto Cu-based metal organic framework (MOF), hybridized with graphene oxide (GO) and functionalized GO for H<sub>2</sub>S removal.

Capture of acid gases (CO<sub>2</sub> and H<sub>2</sub>S) at ambient temperature on solid adsorbents was examined by Jeewan Pokhrel et al. 2018 [21] using various metal organic frameworks (MOFs) bearing Cu- and Zr- metal clusters and their composites with graphene oxide (GO)

Cadmium-based materials with varying hydroxide to carbonate ratios and their composites with graphite oxide were synthesized and then used as H<sub>2</sub>S adsorbents at ambient conditions in the dark or upon a visible light exposure. While the incorporation of a graphene-based phase slightly decreased the extent of the improvement in the H<sub>2</sub>S adsorption capacity in moist conditions caused by photoactivity, its presence in the composites enhanced the performance in dry conditions [22].

Sorption enhancement properties are expected when using rGO graphene oxide in its chemically reduced state. rGO possesses a very high surface-to-volume ratio as well as remaining oxygenated groups. These oxygen-containing functional groups can act as anchoring sites for different metal oxide nanoparticles that can be easily doped by different compounds. For these reasons, rGO constitutes an ideal support for developing nanocomposites that can be used as highly efficient catalysts and sorbents with superior performance respect to other conventional materials.

Recent literature has shown the suitability of combining selective adsorbents with rGO or GO based materials to further improve the adsorption capacity of hydrogen sulfide with respect to the use of pure compounds. Decorating graphene embraces a large variety of molecules

including NH radicals [23], benzenesulfonic acid [24], nitrides [25] and mostly metal (hydr)oxides [19,20,26–34]. In general, the best performances have been obtained with composites combining graphene material with zinc (hydr)-oxide [26–31]. The enhancement of hydrogen sulfide adsorption capacity is due to the specific features of rGO surface that increase the chemical heterogeneity, angle disorder and dangling bonds which contribute to extent the dissociation of H<sub>2</sub>S and to acid-base reactions [30,32]. In addition, oxygen-containing groups anchor metal oxy(hydr)oxides preventing aggregation effects and facilitate electron transfer leading to activation of oxygen by the formation of superoxide ions [27,28,31]. Adsorption capacity is also dependent on the graphene material percentage increasing H<sub>2</sub>S adsorption at higher rGO or GO weight percentage [28]. Furthermore, performance can be significantly improved by the incorporation of noble metal nanoparticles because of the increasing number of active groups for initial adsorption of H<sub>2</sub>S [30,33]. Furthermore, the experimental conditions, especially the annealing temperature and time, determine some of the most important features related with the catalytic activity of the composites such as reduction degree of rGO, crystallinity of metal oxides, nanoparticles size, pore-size and surface area [35–38].

Masoud Khaleghi Abbasabadi et al., [24] investigated the removal of H<sub>2</sub>S at low temperature by benzenesulfonic acid-grafted graphene (BS-rGO) nanoadsorbents. An increase of temperature, 30–70 °C significantly improved the adsorption capacity of the nano-adsorbent at 4000–6000 h<sup>-1</sup> space velocities and 60,000 ppm H<sub>2</sub>S feed concentrations.

Despite the good number of studies looking into removal of hydrogen sulfide removal with graphene materials, to the authors' knowledge very little investigation has been conducted on hydrogen sulfide removal at intermediate temperature using zinc oxide sorbents supported on graphene. It is worth mentioning the study on H<sub>2</sub>S adsorption at 300 °C using composites of zinc oxide with reduced graphite oxide (rGO) published by Song et al 2013 [29]. Adsorbents were synthesized using the microwave-assisted reduction method. ZnO/rGO composite showed almost four times higher ZnO utilization efficiency than ZnO itself [29].

Therefore, the aim of this work is to synthesise a new family of reduced graphene ZnO-NiO sorbents (Zn-Ni-rGO) and conduct a preliminary study to explore and assess their potential use for hydrogen sulfide removal at intermediate temperature in order to contribute to the development of gas cleaning for the syngas related sector. In addition, different experimental conditions were applied during the synthesis stage in order to study its effects on the removal capacity of the resulting sorbents.

## 2. Materials and methods

### 2.1. Synthesis of graphene-based sorbents

#### 2.1.1. Graphite oxide

Graphite oxide was synthesized by oxidation of graphite using two different methods: the conventional Hummers method (GrO-H) [39] and the improved Tour method (GrO-T) [40].

For GrO-H preparation, 3 g of graphite powder (<20 μm, Aldrich) and 1.5 g of NaNO<sub>3</sub> were mixed with 70 mL of concentrated H<sub>2</sub>SO<sub>4</sub> and put into an ice bath. The mixture was stirred on a magnetic plate and 9 g of KMnO<sub>4</sub> were slowly added in small amounts to keep the reaction temperature below 10 °C. After stirring for 1 h, the ice bath was removed and the temperature increased up to 35 ± 2 °C keeping the stirring for another 2 h. Subsequently, 230 mL of ultrapure water of a resistivity of up to 18.2 MΩ were added producing a highly exothermic reaction reaching 90 ± 5 °C and keeping stirring for 1 h. Shortly, 50 mL of 30 % H<sub>2</sub>O<sub>2</sub> and 200 mL ultrapure water were added resulting in a brilliant yellow color along with bubbling. The obtained yellow-brown suspension was then cooled down to room temperature, allowed to settle overnight. The clear supernatant was decanted and the remaining

**Table 1**  
Experimental conditions for Zn-Ni-rGO sorbents.

Sorbent	Experience	GO synthesis route	Zn(NO <sub>3</sub> ) <sub>2</sub> (g)	Ni(NO <sub>3</sub> ) <sub>2</sub> (g)	Urea (g)	Reduction (T, t)	Annealing (T, t, atmosphere)
rGO1	Zn-Ni-rGO (1)	Hummers	5.84	0.92	1	120 °C, 24 h	250 °C, 24 h, air
rGO3	Zn-Ni-rGO (3)	Tour	5.84	0.92	1	120 °C, 24 h	250 °C, 2 h, Ar
rGO4	Zn-Ni-rGO (4)	Tour	2.92	0.46	1	120 °C, 24 h	250 °C, 2 h, Ar
rGO5	Zn-Ni-rGO (5)	Tour	5.84	0.92	1	120 °C, 24 h	400 °C, 24 h, Ar
rGO	rGO	Hummers	–	–	–	120 °C, 24 h	400 °C, 24 h, Ar

mixture was filtered and washed successively, with 250 mL 1 M HCl and ultrapure water until pH of the supernatant achieved 6–6.5. Finally, the solid graphite oxide was dried by lyophilization.

GrO-T was prepared by mixing 3 g of graphite powder with 18 g of KMnO<sub>4</sub>. 400 mL of a mixture of H<sub>2</sub>SO<sub>4</sub>/H<sub>3</sub>PO<sub>4</sub> (9:1 vol ratio) were added. Then, the mixture was stirred at 50 °C for 16 h changing its color from dark purplish to dark brown. 400 mL of ice milliQ water and 10 mL of 30 % H<sub>2</sub>O<sub>2</sub> were added to finish the oxidation reaction resulting in a bright yellow suspension. Acidic supernatant was decanted and supernatant removed. The obtained GrO-T was washed and dried similarly to GrO-H.

### 2.1.2. Synthesis of ZnO- NiO- rGO sorbents

5 mg.mL<sup>-1</sup> homogeneous dispersions with a total volume of 120 mL of both GrO-H and GrO-T were prepared. Then, dispersions were successively sonicated in a low power sonication bath for 1 h and with probe sonication for 1 h yielding stable and well dispersed graphene oxide (GO) dispersions. Different quantities of Zn(NO<sub>3</sub>)<sub>2</sub>.6H<sub>2</sub>O (99% pure), Ni(NO<sub>3</sub>)<sub>2</sub>.6H<sub>2</sub>O (99% pure) and urea (Table 1) were successively added to the GO dispersions while stirring. Hydrothermal method was used to reduce graphene oxide and to produce the corresponding composites. The mixtures of GO and metal oxide precursors were transferred into PTFE-lined stainless steel autoclaves and subjected to 120 °C for 24 h. The obtained products were washed two times with ultrapure water and dried at 60 °C under vacuum. Finally a thermal annealing treatment to obtain the ZnO-NiO decorated rGO, was performed at different experimental conditions using a tube furnace. For comparison purposes, rGO similar to that in the composites was also synthesized.

The commercial Z-Sorb™ sorbent was selected as reference material for comparison studies. It consists of zinc oxide and nickel oxide as a promoter supported on a proprietary matrix designed to provide stability and prolong the sorbent life.

### 2.2. Test rig

Testing was carried out in a Microactivity Pro Unit. It is a fully automated laboratory scale unit to assess the performance of catalysts and sorbents. A full description of the system can be found elsewhere [41].

The maximum operating gas flow rate is 4.5 NL/min and the unit can work at up to 700 °C and 30 bar. The gas blending system consists of three mass flow controllers to produce the desired mixture composition. When necessary, water or liquid solutions are fed by a piston pump (Gilson 307) and vaporized before entering the reactor. Dry gas and water are preheated separately, in two independent loops. To this aim the entire set-up is housed in a forced air circulation oven maintained at 190 °C.

An inert, sulfur-resistant tubular reactor of OD 9.2 mm and 300 mm long was used for the sulfidation tests. The reactor was placed in a one single zone SS304 oven, which is able to heat the reactor up to 700 °C. Reaction temperature was measured and controlled by a 1.5 mm thermocouple.

For the tests presented in this work the liquid feeding system was not used and nitrogen and a mixture of hydrogen sulfide (9000 ppmv) in nitrogen were fed to the system for the heating and sulfidation stage respectively.

Feed and exit gas stream composition were measured by gas chromatography using a CP4900 Varian gas micro-chromatograph equipped with two columns, a Porapack HP-PLOT Q and a Molecular Sieve HP-PLOT and with two thermal conductivity detectors. To monitor hydrogen sulfide concentration a fast response analysis method was developed using the Porapack channel only. Sampling was carried out in automatic mode and method run time was 3 min. The analysis conditions were: T injector, 106 °C; T column, 100 °C, isothermal; Initial Pressure, 22 psi; mode, constant pressure.

### 2.3. Characterization techniques

The elemental composition of the samples was determined by wavelength dispersive X-ray fluorescence spectrometry (WDXRF) employing an AXIOS automated X-Ray Fluorescence spectrometer (PANalytical) equipped with a 4 kW Rh tube. Samples were pressed into thick pellets of 27 mm diameter. The pellets were analysed with a semiquantitative (OMNIAM) method developed by PANalytical.

The X-Ray Diffraction (XRD) patterns were obtained using X' Pert PRO diffractometer (PANalytical) with Cu-Kα (λ = 1.54 Å) radiation. To determine the bulk mineralogy, randomly oriented powder of each sample was analyzed from 10 to 120° 2θ at a speed of 0.02° 2θ/s. A current of 45 mA and a voltage of 40 kV were employed as tube settings. Phase identification was obtained by the comparison method using the HighScore Plus software (PANalytical) and the Inorganic Crystal Structure Database (ICSD).

The total content of elemental carbon, C was determined by combustion employing a Leco CS 244 instrument.

The morphological analyses of the prepared materials were carried out using a FEG-Nova Nano SEM 230 scanning electron microscope (SEM) equipped with a field emission gun.

Brunauer-Emmett-teller (BET) method was applied to the as-prepared materials to evaluate the specific surface area of graphene samples using an ASAP 2020 analyzer (Micromeritics). It was also employed to evaluate the pores volume of each sample.

### 2.4. Experimental approach

Reduced graphene ZnO-NiO sorbents (Zn-Ni-rGO) were prepared as powder. In order to avoid excessive pressure drop in the reactor, materials were pelletised, weighed and sieved so that the 0.5–1 mm fraction was chosen for testing. The commercial zinc oxide sorbent was originally in cylindrical pellets, so it was ground and re-pelletised similarly to the graphene materials.

Bulk density of the testing-ready sorbents was measured and the sorbent was loaded into the sorbent cage. Depending on the bulk density of the sample from 2 to 4 g were used for testing so that gas hourly space velocity was maintained at 3500 h<sup>-1</sup>.

The reaction system was assembled, and pressurized, checking that there were no gas leaks and heated to the desulfurization temperature with a continuous flow of nitrogen through the reactor. On reaching the desired temperature, the feed gas was switched to the hydrogen sulfide-nitrogen mixture and the sulfidation stage began.

Inlet and outlet gas composition was continuously determined by micro-GC and sulfidation proceeded until the breakthrough point was achieved, that is a sharp increase of hydrogen sulfide concentration at

**Table 2**Elemental analysis of Zn-Ni-rGO sorbents and Z-Sorb<sup>TM</sup> before reactive adsorption.

Element	rGO wt. (%)	Zn-Ni-rGO (1) wt. (%)	Zn-Ni-rGO (3) wt. (%)	Zn-Ni-rGO (4) wt. (%)	Zn-Ni-rGO (5) wt. (%)	Z-Sorb <sup>TM</sup> wt. (%)
C	87	13	12	17	11	–
Ni	–	4,1	3,4	5,5	4,9	5,5
Zn	–	49	40	32	55	34
O	11.4	39	41	45	29	35
Si	–	0.045	0.083	0.061	0.035	15
S	–	0.12	0.19	0.13	0.082	0.067

the reactor outlet. For some tests the sulfidation stage was continued until full sulfidation, i.e. when the hydrogen sulfide concentration at the reactor outlet approached the inlet concentration, which provides information on the slope of the breakthrough curve.

When the sulfidation stage finished, the flow of sulfur gas was stopped and switched to nitrogen to purge and cool down the system under atmospheric pressure. At the end of each run the used sorbent was discharged from the reactor, weighed and characterized.

### 3. Results and discussion

The present study included the selection of commercial ZnO-NiO sorbents (Z-Sorb<sup>TM</sup>) and the synthesis of novel Zn-Ni-graphene sorbents, the assessment of their performance for removing hydrogen sulfide at intermediate temperature and the characterization of the as synthesized, fresh materials, and post-reaction samples.

#### 3.1. Characterization results: Fresh sorbents

The total concentration of the elements present in each sample, after the synthesis, as determined by XRF, are shown in Table 2.

Z-Sorb<sup>TM</sup> proved to be an efficient sorbent for H<sub>2</sub>S removal at intermediate temperature as reported elsewhere [1,2], so, the synthesis of reduced graphene oxide nanocomposites (Zn-Ni-rGO) was made to obtain ZnO and NiO concentrations equal to those of Z-Sorb<sup>TM</sup> in sample 4, and double in samples 1, 3 and 5. For comparison purposes, bare, unfunctionalized rGO similar to that in the composites was also synthesized and studied.

The sorbents prepared with double amounts of Zn(NO<sub>3</sub>)<sub>2</sub> and Ni(NO<sub>3</sub>)<sub>2</sub> (samples 1, 3 and 5) present Zn and Ni concentrations in the range of 40 % to 55 % and 3,4 % to 4,9 % respectively. The sample Zn-Ni-rGO (4) has very similar Zn and Ni concentration to the Z-Sorb<sup>TM</sup> material. Also the concentration of carbon in Zn-Ni-rGO (4) (17 %) is

similar to the concentration of silicon in Z-Sorb<sup>TM</sup> (15 %) both of which are elements constituting the support material.

It is noteworthy that Zn-Ni-rGO (4) presents higher Ni content than the other graphene-based sorbents, despite having been prepared from a solution containing much less nickel. As reported in the preparation section, Zn(NO<sub>3</sub>) and Ni(NO<sub>3</sub>) were added successively to the GO dispersions and subsequently treated hydrothermally to produce the corresponding composites. Looking at the final nickel content in the four sorbent formulations, zinc seems to somehow prevent nickel from grafting to graphene oxide, since all four formulations contain similar final nickel content. Moreover, despite having been prepared with the same amount of Zn(NO<sub>3</sub>) and Ni(NO<sub>3</sub>) precursors, the other three formulations, rGO(1), rGO(3) and rGO(5), show varying content of Zn in the final sorbent, rGO(5) > rGO(1) > rGO(3). Looking at the preparation conditions, longer time for annealing apparently yields higher content of zinc and nickel, with annealing under argon proving slightly better than under air. The sample rGO(3), annealed under shorter time, 2 h and inert atmosphere Ar, shows the lowest zinc and nickel content, but the highest oxygen content.

Oxygen content deserves attention. Sorbents rGO(3) and rGO(4) show higher content when compared to rGO(1) and rGO(5). That may be an indication that most zinc and nickel must be present in the active state for desulfurization, which is as the corresponding oxides.

Fig. 1 shows the XRD patterns of Z-Sorb<sup>TM</sup> and Zn-Ni-rGO nanocomposites before reactive adsorption. As can be observed, an amount of graphene oxide without converting to rGO present in the peak near to 10° (2θ) corresponding to graphene oxide (GO) [6]. In sample 4 the peak corresponding to GO is higher than in samples 1 and 3. Samples 1 and 2 are prepared by Hummers method and samples 4 and 5 by Tour method. These results suggest that the reduction to rGO is more effective after the applied Hummers method or/and in a conventional furnace. The XRD pattern corresponding to Zn-Ni-rGO (5) has a more crystalline profile due to more energetic annealing conditions.

The results of the crystalline characterization by XRD technique showed a very similar composition in the four Zn-Ni-rGO samples, as it is shown in Fig. 1. The patterns confirm that most of the diffraction peaks correspond to the standard data for ZnO structures. The graphene peak is in the range of 23°–25° (2θ) which is not easily visible due to the intensity of the ZnO diffraction peaks. Since there exists no shift in or elimination of characteristic peaks of ZnO (its crystalline structure is preserved) it could indicate that ZnO nanoparticles have not been covalently attached to the graphene sheets [3], then ZnO nanoparticles could cover the surface of graphene sheets [4].

Unfortunately, no diffraction peaks corresponding to NiO structures were revealed except in Zn-Ni-rGO (5) and Z-Sorb samples, but

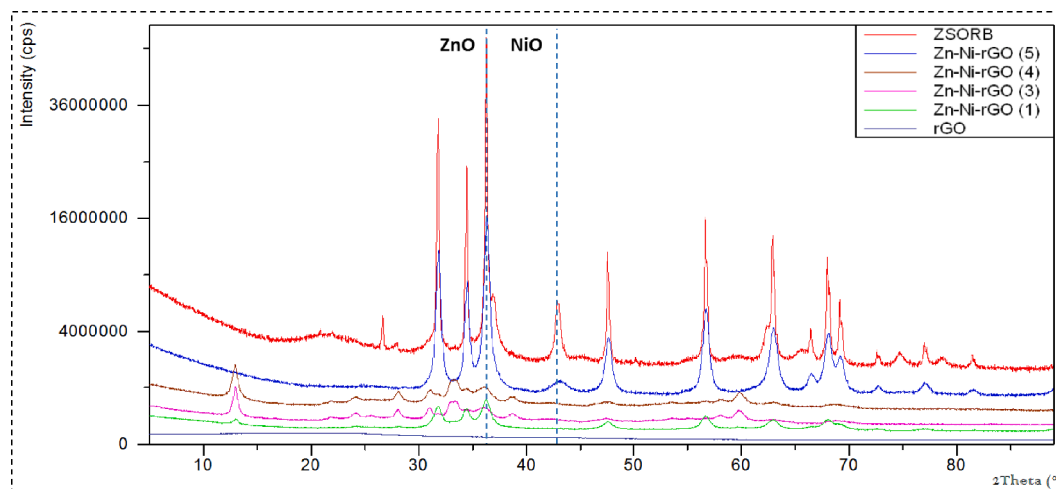


Fig. 1. XRD patterns of Z-Sorb<sup>TM</sup> and Zn-Ni-rGO sorbents before reactive adsorption.

**Table 3**

Textural properties of Z-Sorb™ and Zn-Ni-rGO sorbents before reactive adsorption.

Sample	Specific surface area (SSA) (m <sup>2</sup> . g <sup>-1</sup> )	t-Plot micropore volume (cm <sup>3</sup> . g <sup>-1</sup> )
Z-Sorb™	26.53	0.0015
Zn-Ni-rGO (1)	99.35	0.0035
Zn-Ni-rGO (3)	39.16	0.0004
Zn-Ni-rGO (4)	38.08	0.0014
Zn-Ni-rGO (5)	46.42	0.0028
rGO	403.54	0.0409

**Table 4**

Operating conditions for sulfidation tests.

Operating conditions		
Reactor temperature	T °C Reactor	400 °C
Pressure	P (bar)	10 bar
Gas hourly space velocity	GHSV h <sup>-1</sup>	3500 h <sup>-1</sup>
Feed gas flow rate	F n.c. (ml/min)	Dependent on bulk density of the sorbent to provide the set GSHV 3500 h <sup>-1</sup>
Sulfidation gas composition	%v/v	H <sub>2</sub> S: 0.9 N <sub>2</sub> : 99.1

All the Zn-Ni-rGO nanocomposites presented higher SSA values than Z-Sorb™ which indicates the suitability of the rGO-based composites as useful adsorbents. Zn-Ni-rGO(3) showed the lowest micropore volume that is markedly lower than the other prepared composites. Higher SSA values were obtained for Zn-Ni-rGO sorbents synthesized with Hummer's method than the corresponding prepared by Tour method. Higher SSA can be attributed to reduction for Zn-Ni-rGO(H) composites to a more extent, largely removing oxygen-containing groups, especially carboxyl and epoxy [42]. As expected, the harsher experimental conditions used for the Tour method lead to a higher oxidized graphite. According to literature, rGO prepared from highly oxidized graphite shows higher adsorption ability because of its higher exfoliation and the presence of oxygen-containing functional groups that provide surface metal capturing sites [42].

Fig. 2 shows SEM images with the different magnifications for two of the obtained sorbents, rGO/ZnO-NiO (3) and rGO/ZnO-NiO(4). Both were synthesized by the Tour method, and using the same reduction and annealing conditions. The difference between them is that after synthesis rGO/ZnO-NiO (3) resulted in a high Zn, low-Ni content whereas rGO/ZnO-NiO(4) is a low-Zn, high Ni content sorbent, as shown by XRF analysis. It can be seen that rGO-NiO-ZnO samples present the similar sheet-like morphologies. That sheet-like structure morphologies formed by abundant ZnO and NiO nanoparticles are self-assembled on both sides of lamellar rGO.

### 3.2. Sulfidation tests

Four reduced graphene ZnO-NiO (Zn-Ni-rGO) sorbents have been studied and compared with a reference desulfurization sorbent.

The synthesized sorbents contain different amount of the active sulfur removal species, i.e. ZnO and NiO and of graphene. For comparison purposes, rGO similar to that in the ZnO-NiO-graphene sorbents was also studied. The commercial Z-Sorb™ sorbent was studied as reference material.

Based on the zinc and nickel elemental composition determined by XRF analysis, the corresponding zinc and nickel oxide content is calculated. This assumes that during the sorbent preparation stage all zinc and nickel precursors are effectively converted into their oxides. RGO is estimated as remaining balance.

Operating conditions to determine the desulfurization capacity of the samples are summarized in Table 4.

Sulfidation of the sorbents was studied in the fixed bed reaction system described in section 2.2. Operating conditions were set at P = 10 bar, T = 400 °C, GHSV = 3500 h<sup>-1</sup>, based on previous works published by the authors [5]. Desulfurization experiments were performed on a gas stream containing 9000 ppmv of H<sub>2</sub>S (y<sub>0</sub>). Feed gas flow rate, F<sub>gas n.c.</sub> was set in order to meet the desired GSHV value.

$$GHSV (h^{-1}) = \frac{F_{gas n.c.} (ml/min)}{V_{sorbent} (ml)} \quad (1)$$

Based on the composition of the sorbents, sulfidation reactions expected to happen are

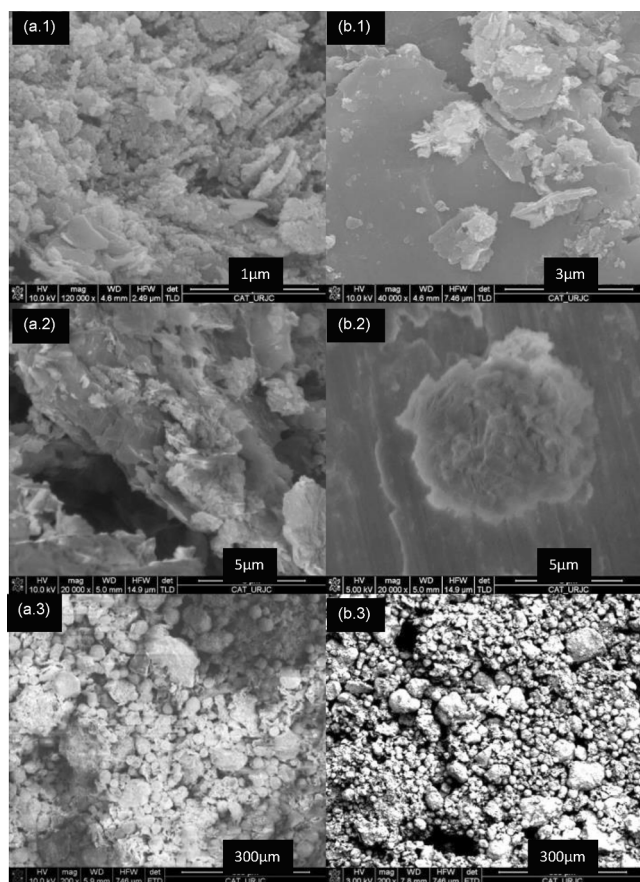


**Fig. 2.** SEM micrographs of the prepared structures based on rGO-NiO-ZnO with different magnifications. (a) rGO/ZnO-NiO (3) a.1) 120.000 Kx; a.2) 20.000Kx y a.3) 300Kx (b) rGO/ZnO-NiO(4) b.1) 40.000Kx; b.2) 20.000Kx y b.3) 300Ks.

elemental analysis shows a great quantity of Ni in the Zn-Ni-rGO nanocomposites from 3.4 % to 5.5 %, indicating the amorphous nature of inorganic phases containing Ni, which can consist probably on Ni oxy(hydr)oxides. There is evidence of amorphous content in the samples, particularly in the samples Zn-Ni-rGO (1), Zn-Ni-rGO (3) and Zn-Ni-rGO (4) as it is shown in Fig. 1. This phenomenon was previously observed in other nanocomposite structures with graphene related materials [5]. This fact could indicate that Ni-compounds nanoparticles have been covalently attached to the graphene sheets.

The specific surface area (SSA) analyses were carried out by physical adsorption of nitrogen (N<sub>2</sub>) at -196 °C and the results were calculated according to the Brunauer-Emmett-Teller (BET) method. Textural properties are reported in Table 3.



The performance of the sorbents has been evaluated by the sulfur level achieved in the reactor exit, and the actual sulfur loading capacity and breakthrough times compared to the theoretical values.

There is ample agreement on the chemistry of hot gas desulfurization by means of sorbents [43]. For a given sulfidation experiment, the concentration of hydrogen sulfide in the product gas is expected to be the equilibrium value as predicted by thermodynamics,  $y = y_{\text{eq}}$ . After a certain time there will be a sharp, continuous increase of hydrogen sulfide leaving the reactor, until the inlet value will be reached. This abrupt change in slope is the breakthrough time, and the concentration against the time curve is called the breakthrough curve. In an ideal reactor, there would be no transport and kinetic limitations, and therefore the breakthrough curve would be the step function  $y = y_{\text{eq}}$  at  $t < t_0$  and  $y = y_0$  at  $t > t_0$ , where  $y_{\text{eq}}$  and  $y_0$  are the equilibrium and inlet mole fractions of hydrogen sulfide respectively, and  $t_0$  the theoretical breakthrough time, that is the time to achieve full sulfidation of the sorbent. Actual reaction systems lead to finite reaction and diffusion rates, axial dispersion and channeling. In practical words, they produce experimental breakthrough curves that are smoothly or sharply sloping. The fractional conversion at the actual breakthrough time provides a measure of sorbent utilisation, while the level of  $\text{H}_2\text{S}$  before breakthrough is also an important measure of sorbent performance.

To determine the performance of the sorbent, equations similar to those used by the authors in their previous research works have been applied. The theoretical sulfur uptake ( $S\text{-upt}_0$ ) (g), on mass basis, for a given sorbent inventory charged into the reactor,  $M_{\text{sorbent}}(\text{g})$ , on reaching full sulfidation will be given by,

$$S\text{-upt}_0 (\text{g}) M_{\text{sorbent}} (\text{g}) * \left( \frac{\text{ZnO}}{100} \frac{AW_S (\text{g})}{MW_{\text{ZnO}} (\text{g})} + \frac{\text{NiO}}{100} \frac{AW_S (\text{g})}{MW_{\text{NiO}} (\text{g})} \right) \quad (2)$$

where  $\text{ZnO}/100$  and  $\text{NiO}/100$  denote the fraction, on mass basis, of the active oxides in the sorbent,  $\text{ZnO}$  and  $\text{NiO}$ ,  $MW$  is the molecular weight of  $\text{H}_2\text{S}$ ,  $\text{ZnO}$  and  $\text{NiO}$ , respectively, and  $AW$  the atomic weight of sulfur. This equation is based on the assumption that 1 mol of  $\text{ZnO}$  ( $MW_{\text{ZnO}}$  (g)) reacts with 1 mol of  $\text{H}_2\text{S}$ , to yield 1 mol of  $\text{ZnS}$  and 1 mol of  $\text{H}_2\text{O}$ , and 1 mol of  $\text{NiO}$  ( $MW_{\text{NiO}}$  (g)) also reacts with 1 mol of  $\text{H}_2\text{S}$ , to yield 1 mol of  $\text{NiS}$  and 1 mol of  $\text{H}_2\text{O}$ .

To convert it to percentage basis, the following equation is used

$$S\text{-upt}_0 (\%) = \frac{S\text{-upt}_0 (\text{g})}{M_{\text{sorbent}} (\text{g})} * 100 \quad (3)$$

The actual sulfur captured by the sorbent ( $S\text{-upt}$  (g)), until a given sulfidation time  $t_s$ , is calculated by the equation

$$S\text{-upt} (\text{g}) = AW_S \frac{PF_{\text{gas}} y_{\text{H}_2\text{S}}}{R_g T} t_s \quad (4)$$

Being  $AW_S$  the atomic weight of sulfur, as the species formed according to the sulfidation reactions,  $P$  the absolute pressure at sulfidation conditions,  $F_{\text{gas}}$  the volumetric gas flow rate at process conditions,  $y_{\text{H}_2\text{S}}$  the inlet  $\text{H}_2\text{S}$  mol fraction,  $R_g$  the universal gas constant and  $T$  the absolute temperature at sulfidation conditions.

This procedure assumes that all sulfur is retained by the sorbent.

Based on the given the experimental conditions, the theoretical time ( $t_0$ ) to achieve complete sulfidation of the sorbent, is estimated straightforwardly as follows

$$t_0 (\text{min}) = \frac{S\text{-upt}_0 (\text{g})}{\left[ AW_S \frac{PF_{\text{gas}} y_{\text{H}_2\text{S}}}{R_g T} \right]} \quad (5)$$

The theoretical time will depend on the operating conditions, initial hydrogen sulfide concentration, sulfidation pressure and temperature, as well as on gas flow rate.

During the experiments the actual breakthrough time is given by

**Table 5**

Summary of experimental results and comparison of desulfurization performance.

Sorbent	rGO (1)	rGO (3)	rGO (4)	rGO (5)	Z-Sorb <sup>TM</sup>	rGO
ZnO %	61	50	40	69	42	
NiO %	5.2	4.3	7.0	6.2	7.0	
rGO %	33.8	45.7	53	24.8	0	100
Sorbent load, $M_{\text{sorbent}}$ (gr)	2.2	2.2	1.7	1.7	3.9	1.34
Bulk density (gr/l)	1.1	1.2	0.86	1.0	0.97	0.64
Synthesis	H	T	T	T		H
Experimental conditions	T (°C)	400	400	400	400	400
	P (bar)	10	10	10	10	10
	$y_0 \text{H}_2\text{S}$ (mol %)	0.9	0.9	0.9	0.9	0.9
	Fgas n.c. (ml/min)	108	96	106	91	216
	GHSV n.c. ( $\text{h}^{-1}$ )	3500	3500	3500	3500	3500
theoretical sulfur uptake ( $S\text{-upt}_0$ ) (%)	26	21	19	30	20	
theoretical breakthrough time ( $t_0$ ) (min)	432	396	240	444	288	
Actual breakthrough time (min)	355	443	225	316	163	
Actual sulfur uptake ( $S\text{-upt}$ ) (%)	22	25	18	22	12	0.91
actual sulfur captured by the sorbent ( $S\text{-upt}$ (g))	0.49	0.55	0.31	0.37	0.45	0.012
Yield (Supt/Supt0) (%)	84	114	96	73	58	

analysing  $\text{H}_2\text{S}$  content at the reactor outlet. Sulfidation breakthrough point was set at 0.01 %v/v. However, the sulfidation run proceeded until almost full sulfidation of the sorbent, i.e.  $\text{H}_2\text{S}$  concentration of the outlet gas reached inlet concentration, except for rGO(5).

Table 5 summarizes the results obtained. Experiments were run at 400 °C and 10 bar. GHSV was kept fixed at 3500  $\text{h}^{-1}$ . Based on the amount of sorbent charged into the reactor and their density, to achieve this value, gas flow-rates ranged from 91 to 113 mL/min (expressed in normal conditions). Given that the reactor diameter is 9 mm, linear gas velocity ranged from 2.39 to 2.96 cm/s at normal conditions or from 0.59 to 0.73 cm/s at process conditions. Given the small velocity differences, no significant effect of this parameter on their performance can be expected, e.g. due to mass transfer resistance, or at least not enough to alter their relative performance.

It must be highlighted that even the bare unfunctionalized reduced graphene sorbent, rGO, showed some capacity for sulfur uptake. Given that that sorbent did not contain any zinc or nickel in its formulation, that are the active species for reactive, chemical adsorption, some physical sorption must have happened despite the temperature, 400 °C, not being favourable for such a process.

Another relevant observation is that all the novel functionalized graphene-based sorbents outperformed the commercial sorbent.

Comparison of the actual sulfur loading capacity and breakthrough times with the theoretical values reveal that actual values achieved were close to or for some cases better than the theoretical ones. Consequently, the fractional conversion or yield at the actual breakthrough time provides a very high sorbent utilisation.

RGO(3) even reached sulfidation capacity higher than the predicted by the stoichiometric amount of zinc and nickel oxide that contains. As stated above, the bare unfunctionalized sorbent was able to capture hydrogen sulfide to some extent. However, it is too small to account for the 14% increase over the stoichiometric value observed for RGO(3). It must be noticed that RGO(3) was annealed under milder conditions than RGO, and also that it had the lowest micropore volume of all samples which might lead to higher sulfur capture by the support, and therefore

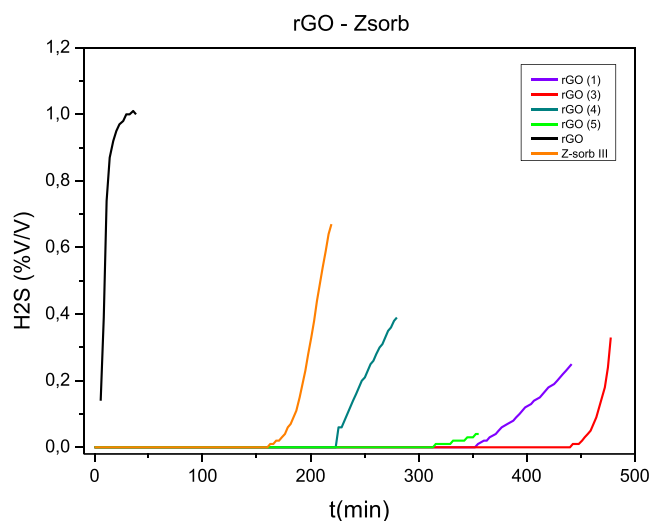


Fig. 3. Breakthrough sulfidation curves ( $T = 400\text{ }^{\circ}\text{C}$ ,  $P = 10\text{ bar}$ ,  $\text{GHSV} = 3500\text{ h}^{-1}$ ,  $\text{H}_2\text{S}$  feed gas = 9000 ppmv,  $\text{N}_2$  balance).

account for the extra sorption capacity.

It is evident that the graphene-based sorbents captured  $\text{H}_2\text{S}$  by an additional mechanism to the main one which is the heterogeneous gas solid chemical reactions of the active species, zinc oxide and nickel oxide with hydrogen sulfide to form the corresponding zinc and nickel sulfides, releasing water vapour. This fact might have gone unnoticed if none of the samples would have reached a capture capacity higher than the theoretical one. Although not fully confirmed, one plausible explanation is that additional hydrogen sulfide was captured by physical sorption, despite being less favourable conditions. One fact that supports this hypothesis is that, during the regeneration runs (not included in this paper) using diluted air ( $\text{O}_2$  3%v/v in  $\text{N}_2$ ), constant sulfur dioxide release was observed. It started at a temperature as low as  $400\text{ }^{\circ}\text{C}$ , way below the expected onset temperature, around  $550\text{ }^{\circ}\text{C}$ , for zinc and nickel sulfide regeneration to proceed in accordance to thermodynamics.

The evolution of hydrogen sulfide at the reactor outlet with time is depicted in Fig. 3. As can be seen, there is almost no  $\text{H}_2\text{S}$  in the exit stream prior to break-through, followed by a sharp increase of the  $\text{H}_2\text{S}$  concentration in the reactor outlet.

The sorbent that yielded the best performance in terms of sulfur retention capacity, rGO(3), also presented the sharpest slope. This is an indication of a steady progress of the reaction front, as is expected for packed bed reactors. The commercial sorbent also showed a sharp sloping curve as did the unfunctionalized rGO sorbent. Sulfidation of the other sorbents resulted in smoother curves. This can be ascribed to some channeling. Particularly, rGO(5), the sorbent to which stronger annealing conditions were applied,  $400\text{ }^{\circ}\text{C}$ , 24 h, under argon atmosphere, showed the smoothest curve. This fact might lead to higher sulfur uptake. Unfortunately, this hypothesis cannot be confirmed because the run was stopped immediately after breakthrough and did not proceed until full sulfidation.

In any case, a trade-off needs to be met between the breakthrough value, the slope of the curve, i.e. the level of hydrogen sulfide that slips the reactor without being trapped, and the overall achievable utilization of the sorbent. This will be dictated by downstream units to the desulfurizer, e.g. gas burner, gas engine, catalytic upgrading and conversion to biofuels or chemicals, etc. In other words, by the end-uses associated with syngas and specifically by their sulfur tolerance level. In practical terms this means that most often the desulfurization sorbents are not brought to full utilization.

The actual hydrogen sulfide picked up by the synthesized sorbents is presented in Table 5. It is noticeable that even the unfunctionalized

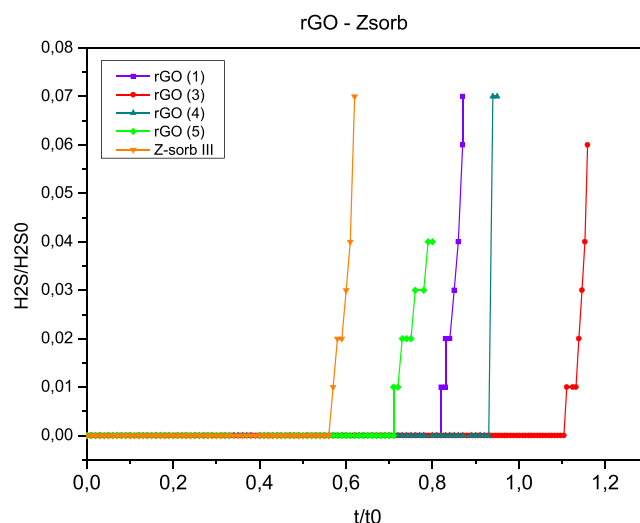


Fig. 4. Dimensionless sulfidation breakthrough curves ( $T = 400\text{ }^{\circ}\text{C}$ ,  $P = 10\text{ bar}$ ,  $\text{GHSV} = 3500\text{ h}^{-1}$ ,  $\text{H}_2\text{S}$  feed gas = 9000 ppmv,  $\text{N}_2$  balance).

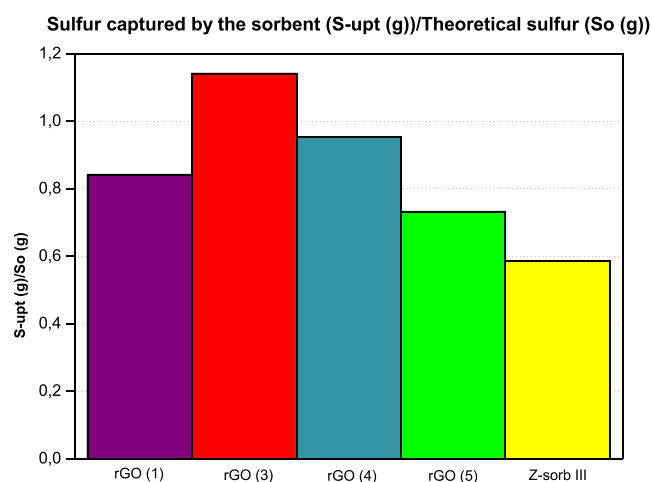


Fig. 5. Comparison of the sorbents in terms of utilization yield ( $T = 400\text{ }^{\circ}\text{C}$ ,  $P = 10\text{ bar}$ ,  $\text{GHSV} = 3500\text{ h}^{-1}$ ,  $\text{H}_2\text{S}$  feed gas = 9000 ppmv,  $\text{N}_2$  balance).

graphene was able to capture some sulfur at the operating conditions studied,  $400\text{ }^{\circ}\text{C}$  and 10 bar. All sorbents were successful in taking hydrogen sulfide away from the gas. The amount of sulfur retained ranges between 0.31 g for rGO(4) and 0.55 g for rGO(3).

Fig. 3 does not allow a straightforward comparison of the novel graphene sorbents among them or with the commercial sorbent. In order to do so the actual data are converted into dimensionless ones.

Thus Fig. 4 shows the evolution of normalized ( $\text{H}_2\text{S}/\text{H}_2\text{S}_0$ ) concentration at the reactor outlet with the normalized time  $t/t_0$ , where  $\text{H}_2\text{S}_0$  is the sulfur content in the feed gas and  $t_0$  is the theoretical time for the complete sulfidation of the metal oxide, as predicted by [eq. (5)].

Dimensionless breakthrough curves allow a straightforward comparison of the performance of the different sorbents.

All graphene-based sorbents performed better than the commercial material studied as reference. Moreover, a very good fractional utilization degree was attained because they reached breakthrough times close to the theoretical ones based on their zinc and nickel content. Actually the best performing graphene sorbent, rGO(3), achieved a longer breakthrough time than predicted theoretically. This indicates that in addition to the active desulfurization components, the support retained some sulfur as well. This hypothesis was confirmed on the unfunctionalized graphene sorbent.

**Table 6**  
Comparative of the graphene supported sorbents studied.

Sorbent	Method	Zn	Ni	Annealing
Zn-Ni-rGO(1)	Hummers	H	H	250 °C, 24 h, air, S
Zn-Ni-rGO(3)	Tour	H	H	250 °C, 2 h, Ar, M
Zn-Ni-rGO(4)	Tour	L	L	250 °C, 2 h, Ar, M
Zn-Ni-rGO(5)	Tour	H	H	400 °C, 24 h, Ar, S
rGO	Hummers	–	–	400 °C, 24 h, Ar, S

Comparison of the performance of the sorbents as yield fractional utilization is presented on Fig. 5. For each material it is established in terms of the ratio of actual sulfur uptake, as calculated by [eq. (4)] to the theoretically achievable sulfur loading for a given sorbent inventory, based on its composition and time on stream, as resulting from [eq. (2)].

Looking at Fig. 5 it is easily noticed that the novel rGO-ZnO-NiO sorbents are able to achieve very good utilization values, higher than 80 % of their theoretical values. They are therefore highly promising as they perform better than the commercial sorbent, under the same operating conditions. The synthesized reduced graphene sorbents differ in (i) graphite oxide synthesis method, (ii) amount of active sulfidation species, Zn and Ni, and (iii) annealing conditions.

To make it easier the analysis of the effect of sorbent preparation procedure on the sulfidation performance, the values from Table 1, have been converted for convenience to give a quick view of the synthesis route (Hummers, H o Tour, T), active species content, (high, H, low, L) and annealing conditions, (strong, S, or mild, M), Table 6.

Strong conditions mean long annealing time, 24 h, potentially oxidizing atmosphere, air, and/or high temperature, 400 °C. Meanwhile, mild conditions are related to short annealing time, 2 h, inert atmosphere, Ar and moderate temperature, 250 °C.

According to the data presented on Figs. 4 and 5, in terms of their performance towards hydrogen sulfide removal at intermediate temperature, the sorbents are rated as follows

$$\text{rGO(3)} > \text{rGO(4)} > \text{rGO(1)} > \text{rGO(5)} > \text{Z-Sorb}^{\text{TM}} > \text{rGO}$$

The most relevant fact is that the four novel graphene-based sorbents presented in this work showed better performance than the commercial ZnO-NiO sorbent studied for comparison. The synergistic effect of rGO can be attributed to the buffer effect against the aggregation of ZnO and NiO nanoparticles, thus improving the performance of rGO-NiO-ZnO composites [44]. In addition, the defect sites on rGO enable the facile desorption of S by rapid electron transfer in redox reactions [45]. This gives them credit for further development and studies of hydrogen sulfide removal at intermediate temperature, applicable to sectors such as syngas cleaning.

Looking at the synthesis conditions of the reduced graphene ZnO-NiO sorbents as presented on Table 6 the following observations can be derived:

Both methods used for the synthesis of the graphite oxide, the conventional Hummers method (GrO-H) and the improved Tour method (GrO-T) led to stable, successful precursors, able to anchor the active species for hydrogen sulfide sorption, ZnO and NiO.

When the sorbents contain similar amounts of the species active for reactive adsorption, ZnO and NiO, annealing under milder conditions, short time, 2 h and inert atmosphere, rGO(3) and rGO(4), seem to lead to better performance than strong annealing conditions, such as long time, and a potentially oxidizing atmosphere, rGO(1). According to the literature, composites calcined at lower temperature contain more surface defects which can enhance the surface activity. [44].

Longer times for annealing at high temperature under non oxidizing atmospheres, 24 h, 400 °C, Ar, rGO(5), does not seem to increase the yield of the sulfur captured. In fact, it performed worse than the other sorbents annealed in argon atmosphere, rGO(3) and rGO(4). However, it is expected that it will provide better stability of the support if subjected to cycling.

Although the unfunctionalized material, rGO, had a certain degree of

**Table 7**  
Elemental analysis of Zn-Ni-rGO sorbents and Z-Sorb<sup>TM</sup> after reactive sulfidation adsorption tests.

Element	rGO	rGO-ZnO-NiO (1) Conc. (%)	rGO-ZnO-NiO (3) Conc. (%)	rGO-ZnO-NiO (4) Conc. (%)	rGO-ZnO-NiO (5) Conc. (%)	Z-Sorb <sup>TM</sup>
C	84	5.1	5.8	5.9	6.3	0.24
Ni	–	3.9	4.1	6.7	4.6	5.3
Zn	–	48	34	34	46	31
O	12	14	15	16	17	25
Si	–	0.044	0.089	0.072	0.054	14
S	0.87	28	28	25	20	15

sulfur capture, ZnO and NiO are obviously needed in the graphene-based sorbent formulation to have a selective sulfur removal sorbent working successfully at intermediate temperature. Contrary to what was expected, higher contents of ZnO and NiO in the formulations, sorbents rGO(1) and rGO(5), do not necessarily increase the ability for sulfur uptake. In fact, rGO(5), which according to XRF analysis had the highest zinc and nickel content, was the worst performing graphene based sorbent. Despite rGO(4) being prepared from lower amounts of Zn(NO<sub>3</sub>) and Ni(NO<sub>3</sub>), which is very relevant from an economic point of view, it resulted in a very promising sorbent, with very good fractional utilization.

In summary, reduced graphene ZnO-NiO nanocomposites (Zn-Ni-rGO) prepared by Tour method at moderate annealing temperature and time showed the highest desulfurization performance compared to the same prepared at harsher conditions (rGO-NiO-ZnO(5)). Lower performance of nanocomposites prepared at higher annealing temperature can be attributed to the loss of epoxy and carboxyl groups that sharply occur from 400 °C [46].

Although reactive adsorption may be the main mechanism for the H<sub>2</sub>S adsorption by the binding of H<sub>2</sub>S molecules to the Ni centers in the graphene layers, the enhancement in H<sub>2</sub>S adsorption can be attributed to physical adsorption of H<sub>2</sub>S in the pore space formed at the interface between the metal oxide units and the graphene layers [47]. H<sub>2</sub>S reaction with the epoxy and carboxylic groups at the edge of the graphene layers can also occur [48].

Higher adsorption capacities were observed for rGO-NiO-ZnO nanocomposites with low crystallinity and moderate SSA (rGO(3)-rGO(4)). Higher specific surface area, rGO(5), rGO(1) did not improve sulfur retention. From the obtained results it can be concluded that the micropore volume does not increase H<sub>2</sub>S adsorption. On the contrary, the best performing sorbent, rGO(3) showed a markedly lower micropore volume than the other graphene-based sorbents. According to the literature, the reactive adsorption of H<sub>2</sub>S on rGO/metal hydroxides can occur via acid-base reactions. Within this mechanism, H<sub>2</sub>S is retained on the surface of the adsorbent via a direct replacement of OH groups and via acid-base reaction with the metals (hydr)oxides by formation of sulfites and sulfates [45]. Hence, the presence of intermediate metallic phases as amorphous Ni oxy(hydr)oxides, which are probably present in the most efficient composites, may favour the acid-base reactions described above.

### 3.3. Characterization results: Post-reaction sorbents

Z-Sorb<sup>TM</sup> and Zn-Ni-rGO used samples were analyzed after reaction by means of XRF and XRD. The aim of the characterization was to determine the nature of the sulfur species formed during the reactive adsorption sulfidation.

The elemental composition distribution of the main species as determined by XRF is shown in Table 7.

As expected a high content of sulfur was observed. All the synthesized Zn-Ni-rGO nanocomposites presented similar S contents ranging from 20 to 28 wt% which are higher than the sulfur content in the Z-sorb<sup>TM</sup> sample. This demonstrates a higher adsorption capacity

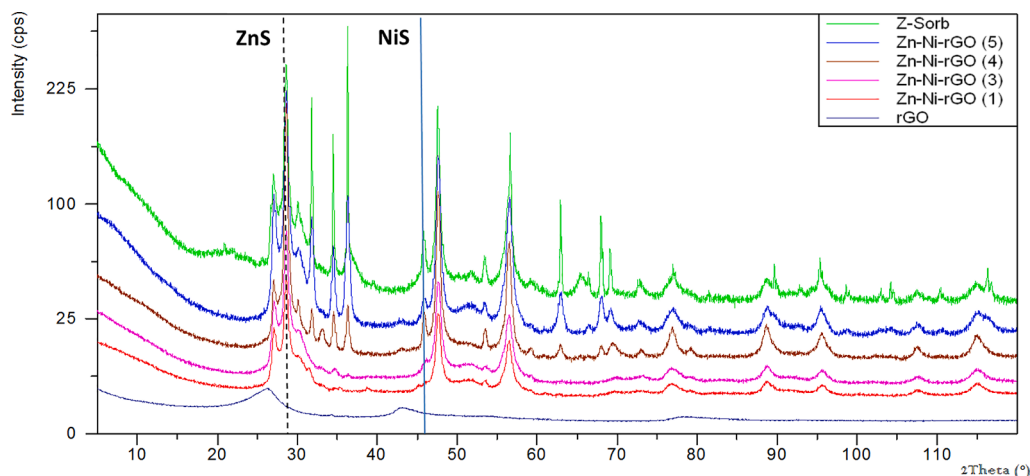


Fig. 6. XRD patterns of Z-Sorb<sup>TM</sup> and Zn-Ni-rGO sorbents after reactive adsorption.

compared to the commercial adsorbent. The enhancement of adsorption capacity is probably linked to the formation of more active sites and porosity due to the interaction between Ni and Zn oxides and the oxygen groups attached to the graphene layers.

Regarding the XRD analyses, after the sulfidation tests at intermediate temperature, 400 °C, the sorbents presented more crystalline profiles as it is shown in Fig. 6. In this case, NiS and NiS<sub>2</sub> phases are shown therefore nickel recovers its crystalline structure.

Zn-Ni-rGO (4) and (5) samples present patterns more like that of the Z-Sorb<sup>TM</sup> sample. Zn-Ni-rGO (1) and (3) show a semi-amorphous structure since fewer peaks than in Zn-Ni-rGO (4) and (5) and Z-Sorb<sup>TM</sup> samples are found but Zn-Ni-rGO (1) and (3) samples do not exhibit any ZnO phase after the sulfidation tests. This seems to imply that for those sorbents all zinc present has been converted to the corresponding sulfide. On the contrary, Zn-Ni-rGO (4) and (5) samples as well as Z-Sorb<sup>TM</sup> showed some zinc remaining as oxide which indicates incomplete sulfidation.

Moreover, no other sulfur species such as sulfites or sulfates are shown by the XRD-analysis, either for the commercial sorbent or for the novel functionalized graphene-based sorbents. Selective sulfidation to yield the corresponding sulfide is a highly desirable feature for a potential sorbent to be applied to syngas cleaning.

The peak near to 10° (2θ) corresponding to graphene oxide (GO) disappears in all Zn-Ni-rGO samples after reaction, perhaps, due to the total reduction of the samples during the temperature and reducing atmosphere to which they have been subjected.

#### 4. Conclusions

In order to contribute to the development of hydrogen sulfide removal at intermediate temperature, new sorbents based on ZnO-NiO on reduced graphene (Zn-Ni-rGO) have been synthesized and their performance assessed on laboratory scale experiments.

Regarding the formulation and preparation of the sorbents, the main conclusions are:

- Conventional Hummers method (GrO-H) and the improved Tour method (GrO-T) produced stable precursors, able to anchor the active species for hydrogen sulfide sorption, ZnO and NiO.
- Subsequent addition of Zn(NO<sub>3</sub>)<sub>2</sub> and Ni(NO<sub>3</sub>)<sub>2</sub> to GO, followed by reduction and annealing produced suitable sorbent formulations for intermediate temperature desulfurization

Regarding performance of the prepared sorbents at laboratory scale, the following conclusions can be drawn:

- They were able to achieve full removal of H<sub>2</sub>S at the process conditions studied, P = 10 bar, T = 400 °C, GHSV = 3500 h<sup>-1</sup>, 9000 ppmv of H<sub>2</sub>S in nitrogen.
- Desulfurization occurred by selective adsorptive reaction of hydrogen sulfide with ZnO and NiO to yield the corresponding sulfides as confirmed by the analysis of post-reaction samples.
- All graphene-based sorbents performed better than the commercial material studied as reference, attaining a very good fractional utilization degree and reaching breakthrough times close to the theoretical ones based on their zinc and nickel content.

In summary, the new family of reduced graphene ZnO-NiO sorbents, Zn-Ni-rGO, synthesized by non-expensive and easily replicable scalable methods, can be a potential candidate for syngas cleaning.

#### Declaration of Competing Interest

The authors declare that they have no known competing financial interests or personal relationships that could have appeared to influence the work reported in this paper.

#### Acknowledgments

The authors wish to thank the Spanish Ministry of Economy, Industry and Competitiveness and the Ministry of Science and Innovation, for the financial support to this research, through the ECOSGAS (Reference ENE2016-75811-R) and GONDOLA (Reference PDC2021-120799-I00) Projects.

#### References

- [1] Prabhansu, Karmakar MK, Chandra P, Chatterjee PK. A review on the fuel gas cleaning technologies in gasification process. *Journal of Environmental. Chem Eng* 2015;3(2):689–702.
- [2] Woolcock PJ, Brown RC. A review of cleaning technologies for biomass-derived syngas. *Biomass Bioenergy* 2013;52:54–84.
- [3] Schmidt R, Tsang A, Cross J, Summers C, Kornosky B. Laboratory simulated slipstream testing of novel sulfur removal processes for gasification application. *Fuel Process Technol* 2008;89(6):589–94.
- [4] Qiu L, Zou K, Xu G. Investigation on the sulfur state and phase transformation of spent and regenerated S zorb sorbents using XPS and XRD. *Appl Surf Sci* 2013;266:230–4.
- [5] Sánchez JM, Ruiz E, Otero J. Selective removal of hydrogen sulfide from gaseous streams using a zinc-based sorbent. *Ind Eng Chem Res* 2005;44(2):241–9.
- [6] Sánchez-Hervás JM, Otero J, Ruiz E. A study on sulphidation and regeneration of Z-Sorb III sorbent for H<sub>2</sub>S removal from simulated ELCOGAS IGCC syngas. *Chem Eng Sci* 2005;60(11):2977–89.
- [7] Geim AK, Novoselov KS. The rise of graphene. *Nat Mater* 2007;6(3):183–91.
- [8] Allen MJ, Tung VC, Kaner RB. Honeycomb carbon: A review of graphene. *Chem Rev* 2010;110(1):132–45.

- [9] Lee C, Wei X, Kysar JW, Hone J. Measurement of the elastic properties and intrinsic strength of monolayer graphene. *Science* 2008;321(5887):385–8.
- [10] Balandin AA, Ghosh S, Bao W, Calizo I, Teweldebrhan D, Miao F, et al. Superior thermal conductivity of single-layer graphene. *Nano Lett* 2008;8(3):902–7.
- [11] Bolotin KI, Sikes KJ, Jiang Z, Klima M, Fudenberg G, Hone J, et al. Ultrahigh electron mobility in suspended graphene. *Solid State Commun* 2008;146(9–10):351–5.
- [12] Steurer P, Wissert R, Thomann R, Mühlaupt R. Functionalized graphenes and thermoplastic nanocomposites based upon expanded graphite oxide. *Macromol Rapid Commun* 2009;30(4–5):316–27.
- [13] Coroş M, Pogăcean F, Măgeruşan L, Socaci C, Pruneanu S. A brief overview on synthesis and applications of graphene and graphene-based nanomaterials. *Frontiers of Materials Science* 2019;13(1):23–32.
- [14] Li X, Yu J, Wageh S, Al-Ghamdi AA, Xie J. Graphene in Photocatalysis: A Review. *Small* 2016;12(48):6640–96.
- [15] Shaari N, Kamarudin SK. Graphene in electrocatalyst and proton conducting membrane in fuel cell applications: An overview. *Renew Sustain Energy Rev* 2017;69:862–70.
- [16] Alonso A, Moral-Vico J, Abo Markeb A, Busquets-Fité M, Komilis D, Puentes V, et al. Critical review of existing nanomaterial adsorbents to capture carbon dioxide and methane. *Sci Total Environ* 2017;595:51–62.
- [17] Yang S, Jiang C, Wei S-H. Gas sensing in 2D materials. *Applied. Physics Reviews* 2017;4(2):021304. <https://doi.org/10.1063/1.4983310>.
- [18] Faye O, Raj A, Mittal V, Beye AC. H<sub>2</sub>S adsorption on graphene in the presence of sulfur: A density functional theory study. *Comput Mater Sci* 2016;117:110–9.
- [19] Daraee M, Ghasemy E, Rashidi A. Effective adsorption of hydrogen sulfide by intercalation of TiO<sub>2</sub> and N-doped TiO<sub>2</sub> in graphene oxide. *J Environ Chem Eng* 2020;8(4):103836. <https://doi.org/10.1016/j.jece.2020.103836>.
- [20] Bhorla N, Basina G, Pokhrel J, Kumar Reddy KS, Anastasiou S, Balasubramanian VV, et al. Functionalization effects on HKUST-1 and HKUST-1/graphene oxide hybrid adsorbents for hydrogen sulfide removal. *J Hazard Mater* 2020;394:122565. <https://doi.org/10.1016/j.jhazmat.2020.122565>.
- [21] Pokhrel J, Bhorla N, Wu C, Reddy KSK, Margetis H, Anastasiou S, et al. Cu- and Zn-based metal organic frameworks and their composites with graphene oxide for capture of acid gases at ambient temperature. *J Solid State Chem* 2018;266:233–43.
- [22] Florent M, Wallace R, Bandosz TJ. Removal of hydrogen sulfide at ambient conditions on cadmium/GO-based composite adsorbents. *J Colloid Interface Sci* 2015;448:573–81.
- [23] Faye O, Eduok U, Szpunar J, Samoura A, Beye A. H<sub>2</sub>S adsorption and dissociation on NH-decorated graphene: A first principles study. *Surf Sci* 2018;668:100–6.
- [24] Khaleghi Abbasabadi M, Rashidi A, Khodabakhshi S. Benzenesulfonic acid-grafted graphene as a new and green nanoadsorbent in hydrogen sulfide removal. *J Nat Gas Sci Eng* 2016;28:87–94.
- [25] Ganji MD, Sharifi N, Ahangari MG. Adsorption of H<sub>2</sub>S molecules on non-carbonic and decorated carbonic graphenes: A van der Waals density functional study. *Comput Mater Sci* 2014;92:127–34.
- [26] Ghayedi A, Khosravi A. Laboratory investigation of the effect of GO-ZnO nanocomposite on drilling fluid properties and its potential on H<sub>2</sub>S removal in oil reservoirs. *J Petrol Sci Eng* 2020;184:106684. <https://doi.org/10.1016/j.petrol.2019.106684>.
- [27] Seredych M, Mabayoje O, Bandosz TJ. Visible-Light-Enhanced Interactions of Hydrogen Sulfide with Composites of Zinc (Oxy)hydroxide with Graphite Oxide and Graphene. *Langmuir* 2012;28(2):1337–46.
- [28] Mabayoje O, Seredych M, Bandosz TJ. Reactive adsorption of hydrogen sulfide on visible light photoactive zinc (hydr)oxide/graphite oxide and zinc (hydr) oxychloride/graphite oxide composites. *Appl Catal B* 2013;132–133:321–31.
- [29] Song HS, Park MG, Croiset E, Chen Z, Nam SC, Ryu H-J, et al. Effect of active zinc oxide dispersion on reduced graphite oxide for hydrogen sulfide adsorption at mid-temperature. *Appl Surf Sci* 2013;280:360–5.
- [30] Giannakoudakis DA, Bandosz TJ. Zinc (hydr)oxide/graphite oxide/AuNPs composites: Role of surface features in H<sub>2</sub>S reactive adsorption. *J Colloid Interface Sci* 2014;436:296–305.
- [31] Ugale AD, Umarji GG, Jung SH, Deshpande NG, Lee W, Cho HK, et al. ZnO decorated flexible and strong graphene fibers for sensing NO<sub>2</sub> and H<sub>2</sub>S at room temperature. *Sens Actuators, B* 2020;308:127690. <https://doi.org/10.1016/j.snb.2020.127690>.
- [32] Mabayoje O, Seredych M, Bandosz TJ. Cobalt (hydr)oxide/graphite oxide composites: Importance of surface chemical heterogeneity for reactive adsorption of hydrogen sulfide. *J Colloid Interface Sci* 2012;378(1):1–9.
- [33] Ovsianyskiy O, Nam Y-S, Tsybaleenko O, Lan P-T, Moon M-W, Lee K-B. Highly sensitive chemiresistive H<sub>2</sub>S gas sensor based on graphene decorated with Ag nanoparticles and charged impurities. *Sens Actuators, B* 2018;257:278–85.
- [34] Ayesb AI, Ahmed RE, Al-Rashid MA, Alarrouji RA, Saleh B, Abdulrehman T, et al. Selective gas sensors using graphene and CuO nanorods. *Sens Actuators, A* 2018;283:107–12.
- [35] Zhang P, Li Z, Zhang S, Shao G. Recent advances in effective reduction of graphene oxide for highly improved performance toward electrochemical energy storage. *Energy Environ Mater* 2018;1(1):5–12.
- [36] Sengupta I, Chakraborty S, Talukdar M, Pal SK, Chakraborty S. Thermal reduction of graphene oxide: How temperature influences purity. *J Mater Res* 2018;33(23):4113–22.
- [37] Ungula J, Dejene BF, Swart HC. Effect of annealing on the structural, morphological and optical properties of Ga-doped ZnO nanoparticles by reflux precipitation method. *Results Phys* 2017;7:2022–7.
- [38] Zhao Y, Zhang L, Wei W, Li Y, Liu A, Zhang Y, et al. Effect of annealing temperature and element composition of titanium dioxide/graphene/hemin catalysts for oxygen reduction reaction. *RSC Adv* 2015;5(101):82879–86.
- [39] Hummers WS, Offeman RE. Preparation of graphitic oxide. *J Am Chem Soc* 1958;80(6):1339.
- [40] Marcano DC, Kosynkin DV, Berlin JM, Sinitskii A, Sun Z, Slesarev A, et al. Improved Synthesis of Graphene Oxide. *ACS Nano* 2010;4(8):4806–14.
- [41] Maroño M, Sánchez JM, Ruiz E, Cabanillas A. Study of the suitability of a Pt-based catalyst for the upgrading of a biomass gasification syngas stream via the WGS reaction. *Catal Lett* 2008;126(3–4):396–406.
- [42] Morimoto N, Kubo T, Nishina Y. Tailoring the oxygen content of graphite and reduced graphene oxide for specific applications. *Sci Rep* 2016;6(1):21715.
- [43] Tamhankar SS, Bagajewicz M, Gavalas GR, Sharma PK, Flytzani-Stephanopoulos M. Mixed-oxide sorbents for high-temperature removal of hydrogen sulfide. *Ind Eng Chem Process Des Dev* 1986;25(2):429–37.
- [44] Chen G, Guan H, Dong C, Xiao X, Wang Y. Effect of calcination temperatures on the electrochemical performances of nickel oxide/reduction graphene oxide (NiO/RGO) composites synthesized by hydrothermal method. *J Phys Chem Solids* 2016;98:209–19.
- [45] Mabayoje O, Seredych M, Bandosz TJ. Enhanced reactive adsorption of hydrogen sulfide on the composites of graphene/graphite oxide with copper (hydr) oxychlorides. *ACS Appl Mater Interfaces* 2012;4(6):3316–24.
- [46] Botas C, Álvarez P, Blanco C, Santamaría R, Granda M, Gutiérrez MD, et al. Critical temperatures in the synthesis of graphene-like materials by thermal exfoliation–reduction of graphite oxide. *Carbon* 2013;52:476–85.
- [47] Petit C, Mendoza B, Bandosz TJ. Hydrogen Sulfide Adsorption on MOFs and MOF/Graphite Oxide Composites. *ChemPhysChem* 2010;11(17):3678–84.
- [48] Petit C, Seredych M, Bandosz TJ. Revisiting the chemistry of graphite oxides and its effect on ammonia adsorption. *J Mater Chem* 2009;19(48):9176–85.